

An inverse approach to determine complex modulus gradient of field-aged asphalt mixtures

Meng Ling · Xue Luo · Fan Gu · Robert L. Lytton

Received: 20 October 2016 / Accepted: 14 February 2017 / Published online: 20 February 2017
© RILEM 2017

Abstract This study develops a new mechanical-based method to determine the complex modulus and modulus gradient of field-aged asphalt mixtures using the direct tension test. Due to the non-uniform aging nature of the field cores, the mechanical responses must be measured at different depths. Meanwhile, the monotonic load is not applied at the neutral axis of the field core specimen due to the modulus gradient, the tensile part of the strain is used and should be separated from the measurement because of the eccentric loading. The modulus gradient parameters, the location of the neutral axis, and the stress distribution are first obtained using the elastic

formulas for a series of loading times. Then the complex modulus is determined using the Laplace transform and the elastic–viscoelastic correspondence principle. An inverse approach and iteration are then proposed by using the pseudo strain to accurately calculate the modulus gradient parameters after the relaxation modulus and reference modulus are determined.

Keywords Field cores · Modulus gradient · Eccentric loading · Corresponding principles · Pseudo strain

M. Ling (✉)
Texas A&M Transportation Institute, CE/TTI Bldg 601C,
3135 TAMU, College Station, TX 77843-3135, USA
e-mail: mengling@tamu.edu

X. Luo (✉)
Texas A&M Transportation Institute, CE/TTI Bldg 508B,
3135 TAMU, College Station, TX 77843-3135, USA
e-mail: xueluo@tamu.edu

F. Gu
National Center for Asphalt Technology, 277 Technology
Parkway, Auburn, AL 36830, USA
e-mail: fzg0014@auburn.edu

R. L. Lytton
Zachry Department of Civil Engineering, Texas A&M
University, 3136 TAMU, College Station,
TX 77843-3136, USA
e-mail: r-lytton@civil.tamu.edu

1 Introduction

The dynamic modulus of asphalt mixtures is a material property and one of the most important inputs in the Pavement Mechanistic-Empirical (ME) Design [1]. It is also used as an indicator for either the level of aging or damage of the asphalt mixtures. Due to its importance, the dynamic modulus has been widely used and well determined for the laboratory-mixed-laboratory-compacted (LMLC) asphalt mixtures. In general, the modulus of the unaged LMLC asphalt mixtures is affected by some factors such as binder type and content, aggregate type and gradation, and mix design. These factors can be well controlled in the laboratory and the field construction. However, when considering the field-aged asphalt mixtures, the effects of field aging process

and non-uniform air void distribution cannot be ignored. On the other hand, the properties of field-aged asphalt mixtures can provide valuable information regarding the pavement condition since they can be used to make maintenance decisions and performance predictions.

In general, the field-aged asphalt mixtures become stiffer after a long-term aging period, which is similar with the LMLC mixtures under the long-term aging in the laboratory. In addition to the long-term aging, there is another unique aging feature for the field cores: non-uniform aging in the pavement depth. It is known that the surface of the asphalt layer suffers from the solar radiation and oxidative aging more than deeper layers, as the oxygen needs time to diffuse through the interconnected air voids into the pavement structure from the surface of the pavement. Thus less carbonyl area is formed at deeper layers due to the less volume of oxygen and contact area. As a result, the modulus at the surface is higher than the other layers, and finally a modulus gradient is developed.

In order to take into account the field aging of asphalt mixtures in the Pavement ME Design, considerable research efforts have been made to either simulate or analyze the field aging in the laboratory, in both binder level and mixture level, or extract binders using the solvent from the field cores then determine the complex shear modulus and phase angle of the aged binders [2]. One of the widely used methods is the AASHTO R30 aging procedure [3]. It has been questioned to be too moderate, which cannot be used to reflect the aging of the asphalt mixtures in the field. Meanwhile, in order to simulate aging in a rational way, it is suggested that for different types of asphalt mixtures such as unmodified and modified mixtures, different aging protocols need to be developed [4]. In addition, the complicated non-uniform aging is even more difficult to be simulated. For the binder extraction method, the viscosity is determined for the extracted aged binders at different pavement depths from the field cores, the viscosity gradient with pavement depth and aging time can also be obtained [5]. However, there is one main problem with this method: some effects such as air void distribution, aggregate gradation, binder absorption, and aggregate-binder interaction on the modulus of the mixtures are not considered [6, 7].

As a result, it is preferred to obtain the material properties of the field cores directly. It is known that

conducting the mechanical tests on the field cores remains difficult mainly due to the geometry compared to the LMLC mixtures specimens. The typical issue is the required dimension for a cylindrical specimen. The thickness of field cores normally ranges from 26 to 100 mm (1 to 4 inches) and even smaller for the overlays, which is insufficient to be used in the standard dynamic modulus test. To overcome this issue, recent studies determine that the thickness for rectangular and cylindrical field core specimens can be as thin as 26 mm (1 inch) for both dynamic modulus test and damage test, and the test results are in the same ranges with those for the standard dimension specimen [8, 9]. This valuable conclusion provides a guide for dealing with those with small specimen geometries such as field cores. In these studies, the tested specimens are obtained from different depths of one original field core, which are used to reflect the modulus distribution along the pavement depth. The traditional uniaxial tension-compression test is then conducted at different temperatures and frequencies to obtain the dynamic modulus master curves of field cores at different depths. However, it should be noted that the aging has been found to be most severe in the top surface especially the top 13 mm (0.5 inch) [5, 10]. The methods mentioned above are actually to measure the average modulus of each field core specimen, which may not be able to capture this gradient feature at top 13 mm.

Under this circumstance, this study presents a new mechanical method to determine the complex modulus and modulus gradient of field cores using the direct tension test. The direct tension test is adopted because of the three key advantages: (1) it is simpler to conduct and only takes less than 1 min for a given temperature; (2) it causes no damage to the specimen if the strain limitation is carefully controlled; and (3) the tensile modulus is determined instead of compressive modulus. It has been shown that the tensile modulus and compressive modulus of asphalt mixtures are different in both the magnitudes and phase angles [11]. However, most tests are conducted in the compression mode [1] and flexion mode [12]. The tensile modulus is necessary, especially for the characterization of various types of cracking in the asphalt pavements. In this study, an inverse approach is proposed to accurately determine the complex modulus and modulus gradient at different temperatures using the elastic theory, pseudo strain concept and elastic-viscoelastic correspondence principle.



This paper is organized as follows. The next section describes the information and preparation for both field core specimens and LMLC specimens. The test protocol to determine the complex modulus and modulus gradient is also discussed. The following section provides detailed derivations and results of the complex modulus and modulus gradient using the inverse approach. The last section summarizes the findings and future work.

2 Direct tension test to measure modulus gradient

The test protocol to measure the complex modulus and modulus gradient is elaborated in this section, which include:

1. The materials for testing, containing asphalt field cores and LMLC mixtures;
2. The configuration and procedure of the direct tension test with a nondestructive monotonically increasing load; and
3. The characteristics of mechanical responses of field cores as well as their comparisons with those of LMLC mixtures.

2.1 Asphalt field cores and LMLC mixtures

The asphalt field cores used in this study include one type of hot mix asphalt (HMA). They are collected from a field project near the Austin Bergstrom airport in Texas. The field asphalt mixtures are fabricated with a PG 70-22 asphalt binder and Texas limestone aggregates. The binder content is 5.2%, the nominal maximum aggregate size is 10 mm (3/8 inch). The detailed mix design and the aggregate gradation can be found in this report [13]. The cores are taken at the center of two lanes of a HMA section at 8 months and 22 months after construction. It is reasonable to assume that the collected cores are not damaged by traffic within this aging period when they are in the field.

In order to demonstrate the features of field cores, laboratory HMA specimens are also fabricated. The parallel tests are performed between the field and LMLC specimens to demonstrate the differences in the measured data. Two air void contents for the laboratory specimens are chosen. The tested LMLC specimens are obtained only from the center of the

compacted cylinder samples for the purpose of having uniform air void distributions through their thicknesses.

All of the original cylinder field cores and LMLC mixtures samples are cut into rectangular specimens 102 mm (4 inches) long and 76 mm (3 inches) wide. The thickness of the rectangular specimen varies from 38 to 51 mm (1.5 to 2 inches) dependent on the thickness of the original field core. The thickness of the LMLC specimens is 38 mm (1.5 inches). Then the steel studs are glued on the top, center and bottom of the specimens for placing linear variable differential transformers (LVDTs). The rectangular field core specimen preparation is shown in Fig. 1. The air void content, thickness and aging time of each field and LMLC specimen are given in Table 1.

After being cut and trimmed in the laboratory, each rectangular specimen is fixed with six LVDTs, as shown in Fig. 2a. The two vertical LVDTs are used to measure the vertical deformations of the top and bottom of the specimen, respectively; another pair attached on the two sides is used to measure the vertical deformations of the center of the specimen. The two horizontal LVDTs are used to measure the lateral deformations of the top and bottom, respectively. This lateral deformation is used to determine the Poisson's ratio of field cores, which will be discussed in a following study. The gauge length is 50.8 mm (2 inches) for each LVDT.

2.2 Direct tension test

The direct tension test is conducted using the Material Test System (MTS) shown in Fig. 2b. A nondestructive monotonically increasing load is applied on the rectangular specimens at 10, 20 and 30 °C at a ramp rate of 0.020 mm/min, respectively. This MTS is an electrohydraulic servo machine. It includes a load cell, a temperature chamber, and is connected to a desktop for reading, saving and analyzing the test results including the load and strains. The MTS is also equipped of ball joints. To keep the specimens intact, the maximum tensile strain is set below 100 microstrains as suggested in the literature [14–16]. This type of LVDT can measure 100 microstrains accurately. It takes approximately 2 h to change the temperature of the specimens from one to another, and it takes approximately 8 h to finish the entire set of the tests for three temperatures. A new set of specimens are put in

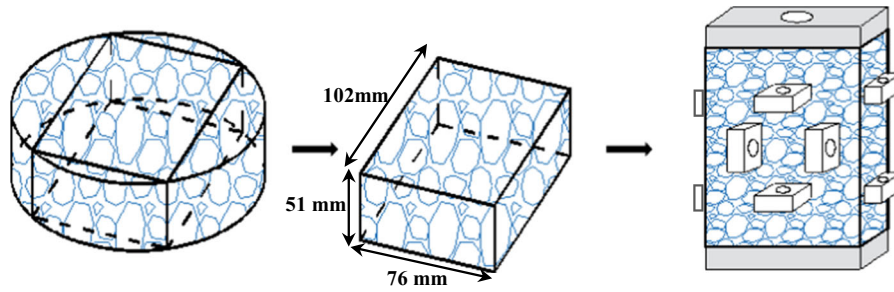
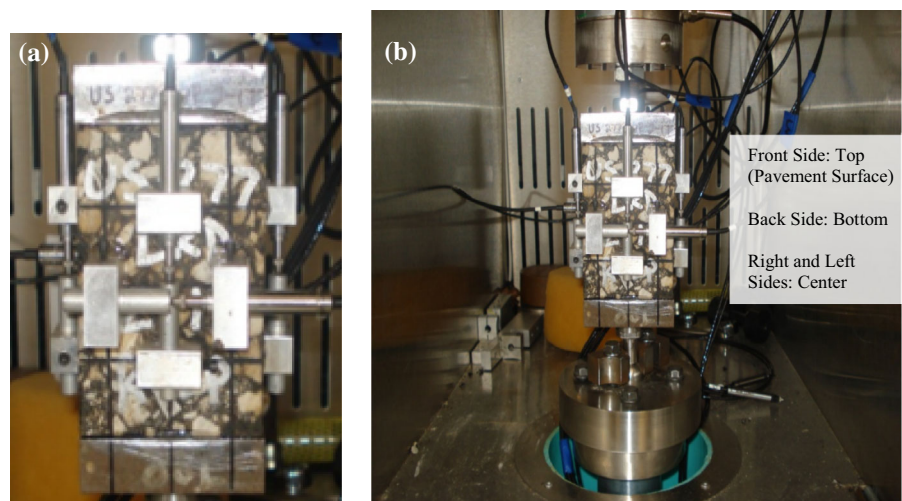


Fig. 1 Field core specimen preparation

Table 1 Field cores and laboratory fabricated mixtures specimens tested in direct tension test

Material type	Air void content (%)	Field aging time (month)	Thickness (mm)
HMA field cores	6.6	8	38
	5.8	8	51
	5.5	22	51
	5.3	22	38
LMLC HMA	6.3	N/A	38
	5.2	N/A	38

Fig. 2 Field core specimen and setup of direct tension test. **a** Specimen with LVDTs. **b** Specimen in the MTS



the temperature chamber overnight to reach the temperature equilibrium and recover the temperature loss due to opening the chamber for unloading and removing the previous specimens.

The direct tension tests conducted on the tested specimens at each temperature are repeated three times in order to avoid the undesired test errors and confirm that the specimens are undamaged during testing. Otherwise, the data cannot be used for analysis. Note that a rest period of 15 min between the two tests is needed to recover the viscoelastic

strains after one test. The three repeated test results are shown in Fig. 3, which indicates that a rest period of 15 min is enough and the repeatability is satisfied.

2.3 Mechanical responses of field cores and LMLC mixtures

The mechanical responses of the field cores and LMLC specimens are discussed herein shown in Figs. 4, 5 and 6. Figure 4a shows the measured loads applied on the field core specimen when the test



Fig. 3 Three repeated test results at 10 °C. **a** Load in three repeated tests. **b** Top and bottom strains in three repeated tests

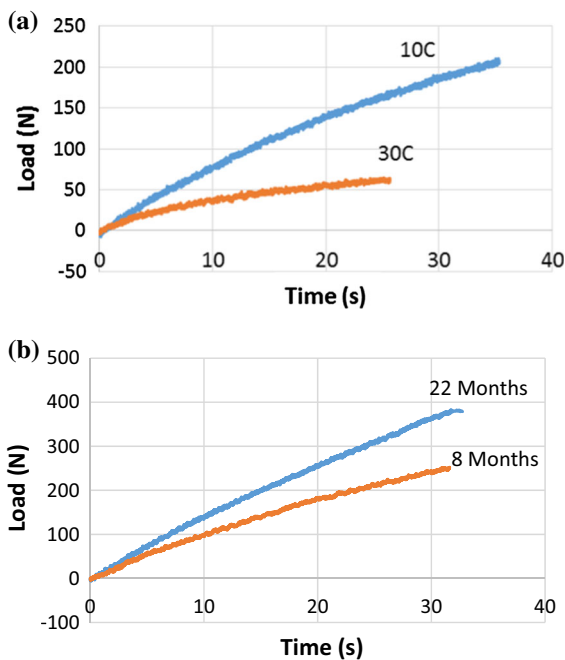
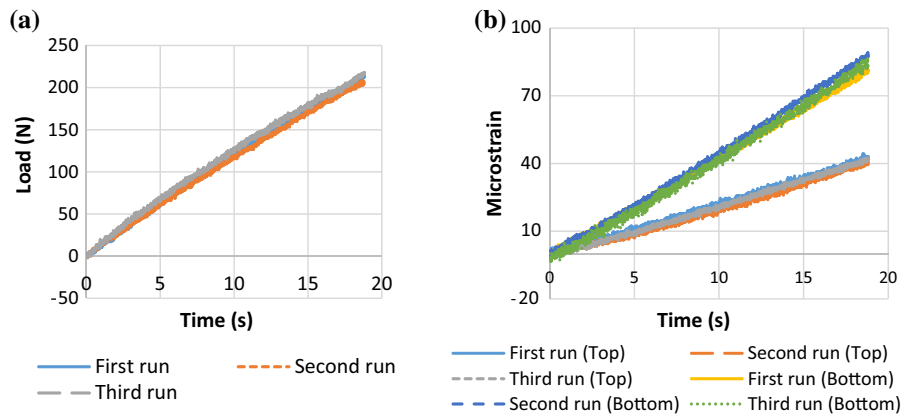


Fig. 4 Monotonic loads in direct tension test. **a** Loads at different temperatures. **b** Loads at different aging times

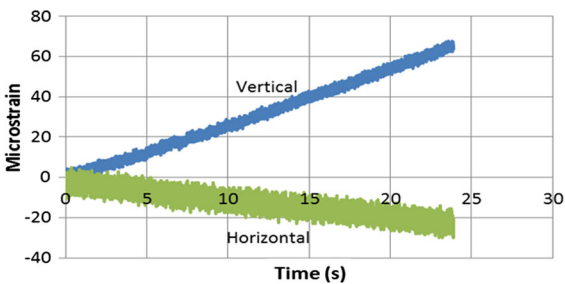


Fig. 5 Measured vertical and horizontal strains at top of field core specimen

temperatures are 10 and 30 °C, respectively. It can be seen that as the temperature increases, the load-time curve becomes smaller and more curved, and the duration of the test is shorter. This observation indicates that the use of time-temperature superposition and thermorheologically simple material properties may be applied to the field specimens. Figure 4b presents the applied loads when the aging times are 8 and 22 months, respectively, it shows when the aging time is longer, the field core specimens become stiffer.

Figure 5 presents the measured vertical and horizontal strains of the field core specimen calculated from the readings of the deformations of one vertical and one horizontal LVDTs attached at the top. The vertical deformations are recorded by the four vertical LVDTs attached at the top, center and bottom, whereas the horizontal deformations are recorded by the two horizontal LVDTs attached on the top and bottom. Note that the vertical strains at the center of the specimen are calculated by averaging the readings from the two LVDTs attached on the two center sides. It is shown that as the tensile load increases, the vertical strain increases whereas the horizontal strain decreases.

Figures 6a and 6b compare the induced vertical strains obtained from the corresponding vertical deformation data for the field core specimen and LMLC specimen, respectively. Under the similar loading, the measured vertical strains in the field and laboratory specimens are obviously different. The three measured vertical strains in the field core specimen (Fig. 6a) have different magnitudes at the three locations, which are closely related to the modulus at each depth. However, the three measured strains for the LMLC specimen are almost identical

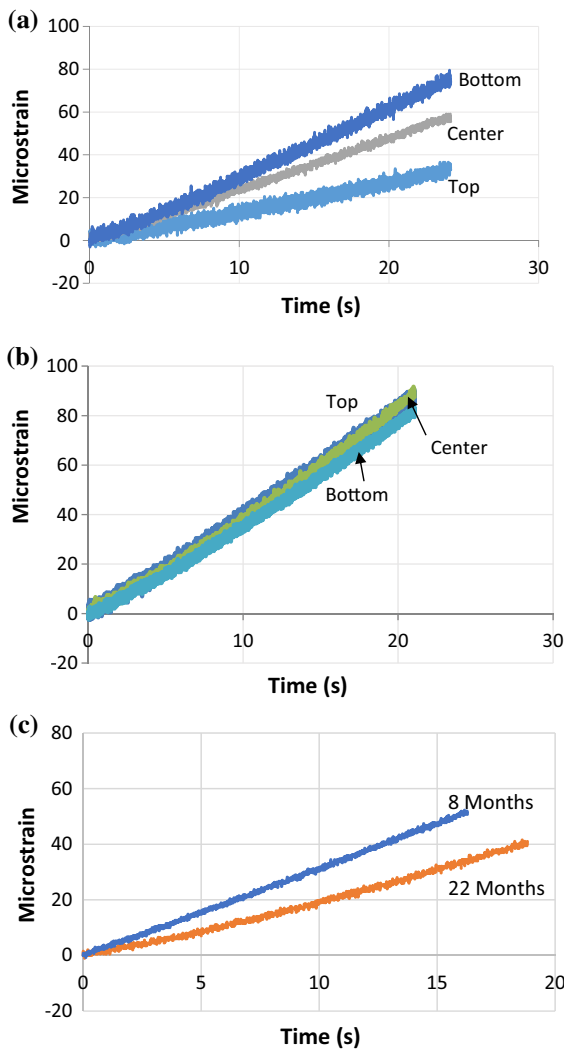


Fig. 6 Measured vertical strains at top, center, and bottom of tested specimen. **a** Strain at different depths of field core specimen. **b** Strain of laboratory fabricated specimen. **c** Strain at different aging times of field core specimen

from Fig. 6b. It is known that the LMLC specimen has an almost uniform modulus across the thickness. Therefore, the difference between three measured strains of the LMLC specimen is minimal. The measured strains at the top, center and bottom for the field core specimens are different, which is due to the non-uniform modulus distribution in the field cores. In general, the strain at the top is smallest and the strain at the bottom is largest, which reflects the modulus distribution. Figure 6c illustrates that the strain is smaller and increases slower for the field

specimen with a longer aging time, which shows the long-term aging effect on the mechanical response.

Due to the existence of the modulus gradient, the monotonic load applied at the center of the field core specimen is actually located different from the neutral axis as shown in Fig. 7. It is expected that the neutral axis is closer to the stiffer side than to the softer side. This eccentricity induces a bending moment and corresponding bending strains at these three locations during the testing. Therefore, the measured strains at the top, center and bottom include two parts: the tensile strain and bending strain. The discussions regarding the eccentric loading are detailed in the next section.

In the previous study [16], the modulus gradient is obtained and verified based on the strain amplitude. As proposed in [16], the modulus gradient of a field core specimen at a specific loading frequency and temperature is modeled by Eqs. (1) and (2):

$$E(z) = E_d + (E_0 - E_d) \left(\frac{d - z}{d} \right)^n \tag{1}$$

$$k = \frac{E_0}{E_d} \tag{2}$$

where $E(z)$ is the dynamic modulus in pavement depth z at a specific loading frequency and temperature; E_d and E_0 are the dynamic moduli at the top and bottom at

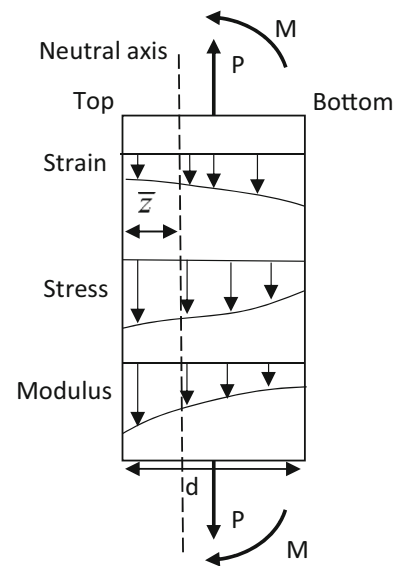


Fig. 7 Illustration of non-uniform distributions of stress, strain, and modulus in field core specimen



the same loading condition, respectively; d is the thickness of the field core specimen; n is the model parameter, which presents the shape of the stiffness gradient; and k is the ratio of the modulus at the top to the modulus at the bottom. When z equals to $\frac{d}{2}$, the center modulus E_c is obtained.

3 Derivations of complex modulus gradient

The objective of this section is to determine the complex modulus based on the unique characteristics of field cores mentioned above. More specifically, there are two main subjects that have to be addressed:

1. How to determine the parameters of the modulus gradient of a field core specimen; and
2. How to convert the measured data and parameters of modulus gradient to its corresponding viscoelastic property: complex modulus.

3.1 Inverse application of viscoelastic-elastic correspondence principle

As stated above, the stress, strain, and modulus of an asphalt field core are non-uniformly distributed as schematically shown in Fig. 7. This adds significant difficulty in the viscoelastic analysis of field core specimens. The solution to this problem is to introduce the viscoelastic-elastic correspondence principle [17], so a viscoelastic problem can be inferred from a reference elastic problem. For an undamaged viscoelastic material, there is a linear relationship between the stress and the pseudo strain:

$$\sigma(t) = E_R \varepsilon^R(t) \quad (3)$$

where $\sigma(t)$ is the stress in the undamaged viscoelastic material, or called viscoelastic stress; $\varepsilon^R(t)$ is the pseudo strain; and E_R is the reference modulus, which can be assigned as the Young's modulus [18]. The pseudo strain is defined as

$$\varepsilon^R(t) = \frac{1}{E_R} \int_0^t E(t - \xi) \frac{d\varepsilon(\xi)}{d\xi} d\xi \quad (4)$$

where $E(t)$ is the relaxation modulus of the material; $\varepsilon(\xi)$ is the strain history; ξ is a time between 0 and t ; t is the loading time. The relaxation modulus for a short

loading time like the one in the direct tension test above can be defined by [19]:

$$E(t) = E_\infty + E_1 e^{-\frac{t}{\kappa}} \quad (5)$$

where E_∞ is the long term relaxation modulus; E_1 is the relaxation modulus coefficient; and κ is the relaxation time.

Once the dynamic modulus of a viscoelastic material is known from the measured load and strain, the relaxation modulus can be calculated from the dynamic modulus-relaxation modulus relationship [20]. Then the reference modulus and pseudo strain can be obtained from Eqs. (3) to (5). The reason why the pseudo strain needs to be determined and used other than the measured strain is that it is not appropriate to use the measured strain which is the viscoelastic strain in the elastic theory (i.e., bending theory) to solve for the modulus gradient parameters n and k . In this study, due to the complexities of stress and strain in the field core specimen, an inverse analysis with an iteration process is proposed to determine the pseudo strain and the gradient parameters. More specifically, it contains the following steps:

I. In the first iteration:

1. Use the measured tensile strain of an undamaged field core specimen as the seed value for the pseudo strain. In other words, temporarily, there is an elastic relationship between the measured stress and the measured strain;
2. Utilize the elastic theory along with the measured load/strains to determine the modulus gradient parameters. The values of n and k are determined and checked for their dependence on loading time and frequency;
3. Convert the functions of the measured load/strains and modulus gradient parameters using the Laplace transform to calculate the corresponding viscoelastic property: complex modulus;
4. Calculate the relaxation modulus then the reference modulus using the calculated complex modulus; and
5. Calculate the pseudo strain by the reference modulus.

- II. In the second iteration: replace the measured strain with the calculated pseudo strain as the seed value after the first iteration and repeat steps 2–5.
- III. In the following iterations (normally 3–5):
 1. Replace the pseudo strain in the previous iteration with the newest one and repeat steps 2–5; and
 2. Stop the iteration when the pseudo strain is stable. Then the modulus gradient parameters converge, the complex modulus and pseudo strain will not change.

In the following subsections, the major steps are elaborated in sequence and the final equations of the complex moduli of different depths of the field cores are presented.

3.2 Determination of modulus gradient parameters

Using the pseudo strain to determine the modulus gradient parameters contains three steps discussed below.

Step 1 Decomposition of vertical strains in field core specimens

As indicated above, there is an eccentricity between the location of the load and neutral axis in the field core specimens. As a result, the vertical pseudo strains at top, center and bottom can be decomposed into the tensile portions and bending portions as follows:

$$\epsilon_0 = \epsilon_{0t} - \epsilon_{0b} = \frac{aP}{AE_0} - \frac{M\bar{Z}}{IE_0} \tag{6}$$

$$\epsilon_c = \epsilon_{ct} + \epsilon_{cb} = \frac{bP}{AE_c} + \frac{M(\frac{d}{2} - \bar{Z})}{IE_c} \tag{7}$$

$$\epsilon_d = \epsilon_{dt} + \epsilon_{db} = \frac{cP}{AE_d} + \frac{M(d - \bar{Z})}{IE_d} \tag{8}$$

where ϵ_0 , ϵ_c , ϵ_d are the vertical pseudo strains at top, center and bottom of the specimen, respectively; ϵ_{0t} , ϵ_{ct} and ϵ_{dt} are the tensile portions of the vertical pseudo strains at top, center and bottom, respectively; ϵ_{0b} , ϵ_{cb} and ϵ_{db} are the bending portions of the vertical pseudo strains at top, center and bottom, respectively; P is the magnitude of the load; and a , b , and c are the coefficients to account for the non-uniform

distribution of the stress in the field core specimen; A is the loading area; M is the induced moment [$M = P(\frac{d}{2} - \bar{z})$]; \bar{Z} is the distance from the neutral axis to the top, $\frac{d}{2} - \bar{Z}$ and $d - \bar{Z}$ are the distances from the neutral axis to the center and from the neutral axis to the bottom, respectively; E_0 , E_c and E_d are the modulus at top, center and bottom, respectively; and I is the moment of inertia. Note that the bending strain at the top is negative, so it is subtracted from the strain at the top as in Eq. (6). At the other two locations, the bending strains are positive.

Step 2 Formulation of value and location of the load in field core specimens.

Assume that the distribution of the tensile portion of the pseudo strain is:

$$\epsilon_t(z) = \epsilon_{0t} + \frac{\epsilon_{dt} - \epsilon_{0t}}{d}z \tag{9}$$

The modulus has a distribution defined in Eq. (1). Then the magnitude of the load is calculated by the integral of the tensile stress as follows:

$$P = m \int_{z=0}^{z=d} \epsilon_t(z)E(z)dz = A \left\{ \epsilon_{0t} \left[\frac{1}{2} + \frac{k-1}{n+2} \right] + \epsilon_{dt} \left[\frac{1}{2} + \frac{k-1}{(n+1)(n+2)} \right] \right\} \times E_d \tag{10}$$

where m and d are the width and thickness of the field core specimen, respectively; and A is the cross sectional area ($A = md$). The location of the neutral axis relative to the top of the specimen is determined by Eq. (11):

$$\bar{Z} = \frac{1}{P} \int_{z=0}^{z=d} mz\epsilon_t(z)E(z)dz = \frac{d \left\{ \epsilon_{0t} \left[\frac{1}{6} + \frac{(k-1)(n+5)}{(n+1)(n+2)(n+3)} \right] + \epsilon_{dt} \left[\frac{1}{3} - \frac{2(k-1)}{(n+1)(n+2)(n+3)} \right] \right\}}{\left[\left[\epsilon_{0t} \left(\frac{1}{2} + \frac{k-1}{n+2} \right) \right] + \left\{ \epsilon_{dt} \left[\frac{1}{2} + \frac{k-1}{(n+1)(n+2)} \right] \right\} \right]} \tag{11}$$

For the case of the LMLC specimen, the pseudo strains are the same at different locations and k equals to 1. Thus \bar{Z} reduces in $\frac{d}{2}$ in Eq. (11), which is the centerline of the specimen. However, for a field specimen, \bar{Z} is always smaller than $\frac{d}{2}$ given that k is larger than 1.



Step 3 Solve for n and k in the modulus gradient model.

Select the values of the pseudo strain and load at different loading times (in this case from 5 to 35 s) of the direct tension test, which are given in Table 2. For every second of the loading time, substitute the measured values into Eqs. (6)–(11) and solve for a , b , c , n , and k . The results of a field core specimen are also given in Table 2. For the first iteration, the values of the pseudo strains are equal to the tensile strains measured from the direct tension test, which are used as the seed values. In the following iterations, these strains are the pseudo strains calculated from the previous iteration after determining the complex modulus and relaxation modulus detailed in the following subsection. The changes of the values of a , b , c , n , and k become small from the second iteration to the third one. Therefore, it is regarded that the results converge at the third iteration. The details regarding the determinations of iterations and pseudo strains will be discussed in the next section.

It should be noted that the exponent n and the ratio k are the material properties since they are the two parameters in the modulus gradient equation and must be included in the application of the correspondence principle which transforms an elastic equation into the Laplace transform of a viscoelastic equation. With each iteration, both n and k are determined to be time-dependent, as seen in Table 2, which shows their final converged values. They both increase slightly with loading time and decreases slightly with frequency.

3.3 Determination of complex modulus using approximated n and k

After obtaining the modulus gradient parameters, the next step is to convert the elastic property to the corresponding viscoelastic property using the Laplace transform. The procedure is given below in sequence.

In the direct tension test, the measured load and tensile portions of the strains versus time of a field core specimen are modeled as follows:

- Monotonic tensile load $P(t)$:

$$P(t) = a_p(1 - e^{-b_p t}) \tag{12}$$

- Tensile portions of the strains at the top and bottom of the field core specimen:

$$\varepsilon_{0t}(t) = a_0(1 - e^{-b_0 t}) \tag{13}$$

$$\varepsilon_{dt}(t) = a_d(1 - e^{-b_d t}) \tag{14}$$

- Modulus gradient parameters n and k :

$$n = n_0 e^{b_n t} \tag{15}$$

$$k = k_0 e^{b_k t} \tag{16}$$

where a_p and b_p are the fitting parameters for the load; a_0 and b_0 are the fitting parameters for the tensile portion of strain at the top; a_d and b_d are the fitting parameters for the tensile portion of the strain at the bottom; and n_0 , k_0 , b_n and b_k are the fitting parameters for the modulus gradient parameters n and k .

Using the Laplace transform, the elastic forms in Eqs. (12)–(16) can be rewritten as viscoelastic

Table 2 Results of calculations of modulus gradient of a field core specimen (8 months aged at 30 °C) from direct tension test

Iteration	Loading time (s)	Pseudo strain ($\mu\varepsilon$)	Load (N)	a	b	c	n	k	n_0	k_0
1st	5–15	6.12	30.41	1.26	0.73	0.85	2.96	2.44	2.54	2.16
	16–25	20.42	165.6	1.28	0.72	0.86	3.73	2.82		
	26–35	34.71	268.34	1.30	0.72	0.87	3.89	3.09		
2nd	5–15	3.67	30.41	1.23	0.70	0.84	2.91	2.40	2.53	2.12
	16–25	12.15	165.6	1.26	0.71	0.85	3.68	2.79		
	26–35	20.3	268.34	1.29	0.71	0.85	3.86	3.06		
3rd	5–15	3.53	30.41	1.22	0.68	0.82	2.90	2.39	2.52	2.11
	16–25	11.79	165.6	1.25	0.70	0.84	3.67	2.76		
	26–35	19.15	268.34	1.27	0.70	0.84	3.85	3.05		



solutions in the Laplace domain by an s-multiplied Laplace transform (Carson transform), which are shown in Eqs. (17)–(21):

$$\bar{P}(s) = \frac{a_p b_p}{s(s + b_p)} \tag{17}$$

$$\bar{\varepsilon}_{0t}(s) = \frac{a_0 b_0}{s(s + b_0)} \tag{18}$$

$$\bar{\varepsilon}_{dt}(s) = \frac{a_d b_d}{s(s + b_d)} \tag{19}$$

$$s\bar{n}(s) = \frac{n_0 s}{s - b_n} \tag{20}$$

$$s\bar{k}(s) = \frac{k_0 s}{s - b_k} \tag{21}$$

where s is the variable in the Laplace domain; $\bar{P}(s)$, $\bar{\varepsilon}_{0t}(s)$, $\bar{\varepsilon}_{dt}(s)$, $\bar{n}(s)$, and $\bar{k}(s)$ are the corresponding load, strains, n and k in the Laplace domain. The viscoelastic forms of n and k are shown in Eqs. (22) and (23). For small values of b_n and b_k , the values of $s\bar{n}(s)$ and $s\bar{k}(s)$ are closely approximated by the constants n_0 and k_0 , as shown in Eqs. (22) and (23).

$$[s\bar{n}(s)]_{s=i\omega} = \left[\frac{n_0 s}{s - b_n} \right]_{s=i\omega} = \frac{n_0 \omega^2 - n_0 b_n \omega}{b_n^2 + \omega^2} \approx n_0 \tag{22}$$

$$[s\bar{k}(s)]_{s=i\omega} = \left[\frac{k_0 s}{s - b_k} \right]_{s=i\omega} = \frac{k_0 \omega^2 - k_0 b_k \omega}{b_k^2 + \omega^2} \approx k_0 \tag{23}$$

To obtain the modulus in the Laplace domain, the Laplace transform is taken on both sides of Eq. (10) and used to solve for the modulus at the bottom, which gives:

$$\bar{E}_d(s) = \frac{\bar{P}(s)}{sA \left\{ \bar{\varepsilon}_{0t}(s) \left[\frac{1}{2} + \frac{k_0 - 1}{n_0 + 2} \right] + \bar{\varepsilon}_{dt}(s) \left[\frac{1}{2} + \frac{k_0 - 1}{(n_0 + 1)(n_0 + 2)} \right] \right\}} \tag{24}$$

where $\bar{E}_d(s)$ is the bottom modulus in the Laplace domain.

The relationship between the complex modulus and relaxation modulus is shown in Eq. (25) [21]:

$$E^*(\omega) = i\omega L\{E(t)\}_{s=i\omega} = [s\bar{E}(s)]_{s=i\omega} \tag{25}$$

Therefore, the complex modulus at the bottom of the field core specimen can be obtained by substituting Eqs. (24) into (25), which is shown by:

$$E_d^*(\omega) = [s\bar{E}_d(s)]_{s=i\omega} = \frac{\bar{P}(s)}{A \left\{ \bar{\varepsilon}_{0t}(s) \left[\frac{1}{2} + \frac{k_0 - 1}{n_0 + 2} \right] + \bar{\varepsilon}_{dt}(s) \left[\frac{1}{2} + \frac{k_0 - 1}{(n_0 + 1)(n_0 + 2)} \right] \right\}}_{s=i\omega} \tag{26}$$

The final expression of the complex modulus at the bottom is shown in Eq. (27) by substituting Eqs. (17)–(19), (22) and (23) into Eq. (26):

$$E_d^*(\omega) = \frac{(AC + BD) + (AD - BC)i}{A^2 + B^2} \tag{27}$$

in which

$$A = \left\{ - \left[\left(\frac{1}{2} + \frac{k_0 - 1}{n_0 + 2} \right) a_0 b_0 + \left(\frac{1}{2} + \frac{k_0 - 1}{(n_0 + 1)(n_0 + 2)} \right) a_d b_d \right] \omega^2 + \left(\frac{1}{2} + \frac{k_0 - 1}{n_0 + 2} \right) a_0 b_0 b_p b_d + \left(\frac{1}{2} + \frac{k_0 - 1}{(n_0 + 1)(n_0 + 2)} \right) a_d b_d b_p b_d \right\} md$$

$$B = \left[\left(\frac{1}{2} + \frac{k_0 - 1}{n_0 + 2} \right) a_0 b_0 (b_p + b_d) + \left(\frac{1}{2} + \frac{k_0 - 1}{(n_0 + 1)(n_0 + 2)} \right) a_d b_d (b_p + b_0) \right] \omega md$$

$$C = a_p b_p (b_0 b_d - \omega^2)$$

$$D = a_p b_p (b_0 + b_d) \omega$$

When the complex modulus at the bottom is determined, the complex modulus at the top in the Laplace domain can be determined as shown in Eq. (28):

$$s\bar{E}_0(s) = sk_0 \bar{E}_d(s) \tag{28}$$

where $\bar{E}_0(s)$ is the corresponding modulus at the top of a field core in the Laplace domain. The complex modulus at the center of the field core in the Laplace domain is determined by:

$$s\bar{E}_c(s) = s\bar{E}_d(s) \left[1 + \frac{k_0 - 1}{2n_0} \right] \tag{29}$$

Similarly, the complex modulus at the top and that at the center can be determined as follows:



$$E_0^*(\omega) = [sk\overline{E_d}(s)]_{s=i\omega} = \frac{k_0(AC + BD) + k_0(AD - BC)i}{A^2 + B^2} \quad (30)$$

$$E_c^*(\omega) = [s\overline{E_c}(s)]_{s=i\omega} = \frac{[1 + \frac{k_0-1}{2^{n_0}}](AC + BD) + [1 + \frac{k_0-1}{2^{n_0}}](AD - BC)i}{A^2 + B^2} \quad (31)$$

The complex modulus includes a real part and an imaginary part, and the dynamic modulus is defined as

$$|E^*(\omega)| = \sqrt{E'^2 + E''^2} \quad (32)$$

where E' is real or storage modulus component; E'' is imaginary or loss modulus component; $|E^*(\omega)|$ is the magnitude of the complex modulus, or dynamic modulus. The phase angle of the complex modulus is calculated using Eq. (33), which is also frequency dependent.

$$\varphi_E = \arctan\left(\frac{E''}{E'}\right) \quad (33)$$

Note that the range of the frequency for the dynamic modulus depends on the duration of the loading time of the direct tension test. A time–frequency relationship is needed to convert the ranges in the time domain to frequency domain. In this study, Eq. (34) is used to make the approximate inverse Laplace Transform based on the [22]:

$$f(t) = [s\overline{f}(s)]_{s=\frac{1}{2t}} \quad (34)$$

The calculated dynamic modulus versus the associated frequency is shown in Fig. 8, using the fitting parameters at the three temperatures.

3.3.1 Determination of complex modulus using complex n and k

It should be mentioned that the calculations of the complex modulus above are based on the approximated results of Laplace transform of n and k by Eqs. (22) and (23). This generates a dynamic modulus gradient, but results in an issue that the phase angles at the top, center, and bottom are the same according to Eqs. (27), (30), (31), and (33). As a matter of fact, the phase angle should also have a gradient along the pavement depth. However, the derivations and computations become too complicated when using the

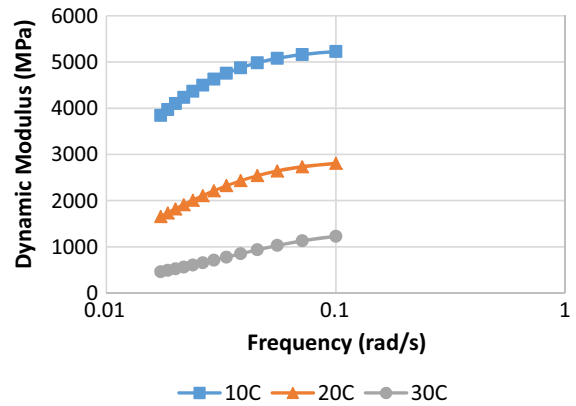


Fig. 8 Calculated dynamic modulus of a field core specimen at three temperatures

accurate results of Laplace transform of n and k . In this study, the approximation method to calculate the complex moduli is adopted. The derivations and expressions of the complex moduli with complex n and k are presented in the Appendix, which also provides the phase angle gradient accurately.

3.3.2 Determination of relaxation modulus, reference modulus and modulus gradient

After obtaining the initial complex modulus, the corresponding relaxation modulus and reference modulus can be computed. First, the master curve of the dynamic modulus is constructed at a reference temperature of 20 °C using the sigmoidal model shown in Eq. (35).

$$\log|E^*(\omega)| = \delta + \frac{\alpha}{1 + e^{\beta + \gamma \cdot \log(\omega \cdot a_T)}} \quad (35)$$

where δ is the value of the lower asymptote, α is the difference between the upper and lower asymptotes, β and γ are shape coefficients, and a_T is the time–temperature shift factor. The Williams–Landel–Ferry (WLF) equation is employed as the shift factor equation:

$$\log a_T = -\frac{C_1(T - T_r)}{C_2 + (T - T_r)} \quad (36)$$

where T is the test temperature, T_r is the reference temperature, C_1 and C_2 are the positive fitting parameters. Figure 9 shows the master curve constructed by Eqs. (35) and (36) for the bottom modulus of a field core specimen.



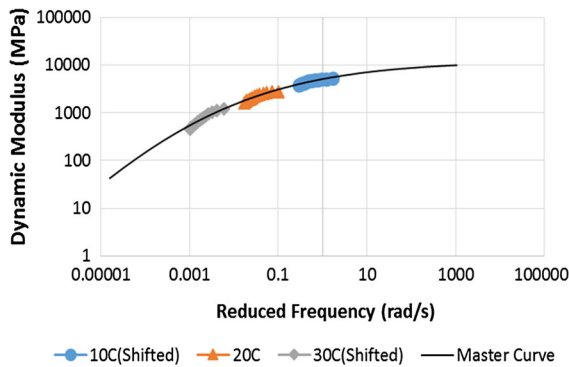


Fig. 9 Dynamic modulus master curve of a field core specimen

Once the dynamic modulus master curve is determined, the relaxation modulus can also be constructed according to their relationships shown in Eqs. (37) and (38). When the relaxation modulus is fitted by the Prony series model:

$$E(t) = E_{\infty} + \sum_{j=1}^M E_j e^{-\frac{t}{\kappa_j}} \tag{37}$$

where E_{∞} is the long term relaxation modulus; E_j are the relaxation modulus coefficients; and κ_j are the relaxation times. The dynamic modulus is given by:

$$|E^*(\omega)| = \sqrt{\left(E_{\infty} + \sum_{j=1}^M \frac{\omega^2 \kappa_j^2 E_j}{1 + \omega^2 \kappa_j^2}\right)^2 + \left(\sum_{j=1}^M \frac{\omega^2 \kappa_j^2 E_j}{1 + \omega^2 \kappa_j^2}\right)^2} \tag{38}$$

As a result, the fitting parameters for the relaxation modulus can be computed by Eq. (38) based on the dynamic modulus master curve determined above. The calculation results is given in Fig. 10.

To facilitate the calculation of the pseudo strain, fit the relaxation modulus determined above by a

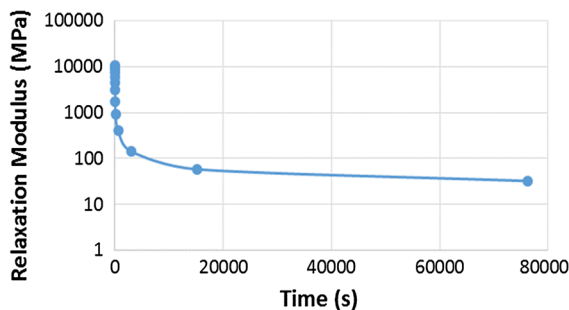


Fig. 10 Relaxation modulus determined from the dynamic modulus master curve

simpler model like that in Eq. (5). Substitute Eq. (5) and the strain history formulated by Eqs. (14) into (4), which gives:

$$\varepsilon_d(t) = \frac{1}{E_R} \left[(E_{\infty} a_d (1 - e^{-b_d t}) + \frac{E_1 a_d \kappa}{\frac{1}{b_d} - \kappa} (e^{-b_d t} - e^{-\frac{t}{\kappa}})) \right] \tag{39}$$

where $\varepsilon_d(t)$ is the pseudo strain at the bottom of the field core specimen. Since the Young’s modulus of asphalt materials is not easy to determine using [18], the representative elastic modulus formulated by Eq. (40) is used to estimate the reference modulus [20].

$$E_R = E_{re} = \frac{1}{2} \left[|E^*|_{f=\frac{1}{t_p}} + E\left(t = \frac{t_p}{2}\right) \right] \tag{40}$$

where E_{re} is the representative elastic modulus; $|E^*|$ is the dynamic modulus; f is the frequency of a load pulse; and t_p is the pulse time of a load. The pulse time of 0.1 s is chosen in this study, so using Eq. (40), the reference modulus is calculated with the dynamic modulus master curve and relaxation modulus determined previously. The pseudo strains at 30 °C at different iterations and the strain measured from the direct tension test are shown in Fig. 11. It can be seen that the pseudo strain is smaller than the measured strain, especially for the longer loading time. This phenomenon matches the understanding that the viscous effect is more active when the temperature is higher, which is corresponding to a lower loading frequency or a higher loading time.

Once the relationships of the pseudo strains and time are determined, the measured strains used in the first iteration are replaced by the pseudo strains to recalculate the values of n and k using Eqs. (6)–(11).

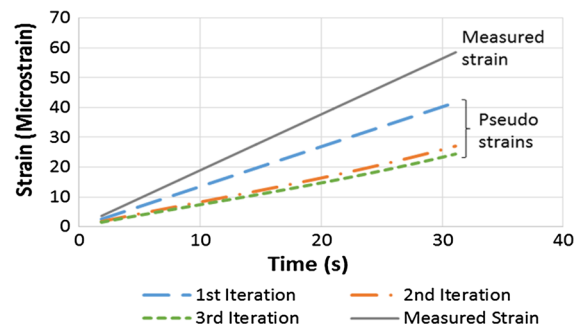


Fig. 11 Measured strain at the bottom of a field core specimen and associated pseudo strains at different iterations



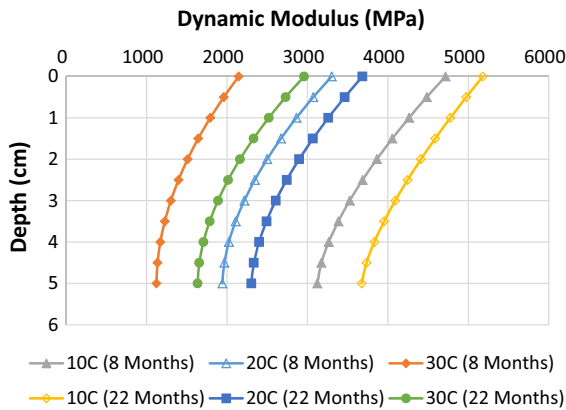


Fig. 12 Modulus gradients of 8 and 22 months aged field specimens at three temperatures and 0.1 Hz

Then the updated values of n and k are inserted into Eqs. (26)–(40) to obtain the new dynamic modulus master curve and relaxation modulus again. This procedure is repeated until the convergence requirement of the values of n and k are met. In general, the values of n and k become stable within 5 iterations. For instance, in Fig. 11, the change of the pseudo strain at 30 °C is minimal after 3 iterations. Once the convergence is reached, the complex modulus and the modulus gradient parameters can be regarded as the actual material properties. The three complex moduli are determined with the updated n and k using Eqs. (27), (30) and (31). The modulus gradient is then extracted from the dynamic modulus curves at the three depths and three temperatures for 8 and 22 months aged field core specimens when the loading frequency is 0.1 Hz, which is shown in Fig. 12.

4 Conclusions and future work

This paper targets the asphalt field cores and proposes a methodology to determine the complex modulus and modulus gradient using the direct tension test. A total of four HMA field cores at two aging times and two laboratory fabricated mixtures are prepared and tested in this study. The major contributions of this paper are summarized as follows:

- The strains at different depths of the field core specimens are different, which is related to the modulus gradient, however, the strains for the LMLC mixtures are almost identical.

- Due to the nature of the modulus gradient, the strains should be decomposed into tensile and bending portions from the elastic theory. The tensile portion is used and the two aging parameters n and k in the modulus gradient equation for different loading times and the modulus gradient can be obtained.
- Using the Laplace transform and correspondence principle, the elastic forms can be further converted into the viscoelastic forms, which is used to determine the dynamic modulus.
- An inverse approach with an iteration process for field cores is proposed using the pseudo strain concept. The relaxation modulus and reference modulus are determined to calculate the pseudo strain. Since the measured strain (i.e., viscoelastic strain) is not appropriate to be used in the elastic formulas, pseudo strain should be calculated to determine the accurate results of n and k , and dynamic modulus.

In a continuation of this paper, the dynamic modulus, viscoelastic Poisson's ratio and the corresponding phase angles will be determined to obtain a full characterization of the viscoelastic properties of asphalt field cores. The viscoelastic properties of the field core specimens are elaborated and show the time-dependency, non-uniform aging dependency and the long-term aging dependency. It is worth noting that the air void distribution of field specimens also has an influence on the dynamic modulus at different depths, and it should be taken into account carefully. In addition, the properties of warm mix asphalt mixtures (WMA) at the same aging condition are compared with the HMA dynamic modulus and Poisson's ratio.

Funding This study was funded by the National Cooperative Highway Research Program (NCHRP) Under Project NCHRP 01-52: A Mechanistic-Empirical Model for Top-Down Cracking of Asphalt Pavement Layers.

Compliance with ethical standards

Conflict of interest The authors declare that they have no conflict of interest.

Appendix

When the accurate Laplace transformed results of n and k are used to derive the complex modulus, the

expressions of A and B in Eq. (27) become different, whereas C and D remain the same since n and k are not involved.

In the new expressions of A and B , the terms with n_0 and k_0 should be replaced by the corresponding forms in the Laplace domain shown in Eqs. (20) and (21); specifically there are two different terms with n_0 and k_0 in A and B that need to be replaced by the complex numbers, which are $\frac{1}{2} + \frac{k_0 - 1}{n_0 + 2}$ and $\frac{1}{2} + \frac{k_0 - 1}{(n_0 + 1)(n_0 + 2)}$.

Therefore, the term of $\frac{1}{2} + \frac{k_0 - 1}{n_0 + 2}$ is determined shown in Eq. (41) using complex numbers of n and k .

$$\frac{1}{2} + \frac{k^*(\omega) - 1}{n^*(\omega) + 2} = \frac{1}{2} + (F_1 + iF_2) \tag{41}$$

where $F_1 = \frac{A_1A_3 + A_2A_4}{A_3^2 + A_4^2}$, $F_2 = \frac{A_1A_4 - A_2A_3}{A_3^2 + A_4^2}$

$$A_1 = (\omega^2 + b_n^2)[\omega^2(k_0 - 1) - b_k^2]$$

$$A_2 = (\omega^2 + b_n^2)b_k k_0 \omega$$

$$A_3 = (\omega^2 + b_k^2)[\omega^2(n_0 + 2) + b_n^2]$$

$$A_4 = (\omega^2 + b_k^2)b_n n_0 \omega$$

Meanwhile, the term of $\frac{1}{2} + \frac{k_0 - 1}{(n_0 + 1)(n_0 + 2)}$ is determined in Eq. (42).

$$\frac{1}{2} + \frac{k^*(\omega) - 1}{[n^*(\omega) + 1][n^*(\omega) + 2]} = \frac{1}{2} + (G_1 + iG_2) \tag{42}$$

where $G_1 = \frac{A_5A_7 + A_6A_8}{A_7^2 + A_8^2}$, $G_2 = \frac{A_5A_8 - A_6A_7}{A_7^2 + A_8^2}$

$$A_5 = [\omega^2(k_0 - 1) - b_k^2](\omega^2 + b_n^2)^2$$

$$A_6 = b_k k_0 \omega (\omega^2 + b_n^2)^2$$

$$A_7 = (\omega^2 + b_k^2)[(\omega^2(n_0 + 1) + b_n^2)(\omega^2(n_0 + 2) + 2b_n^2) - b_n^2 n_0^2 \omega^2]$$

$$A_8 = b_n n_0 \omega [(\omega^2(n_0 + 1) + b_n^2) + (\omega^2(n_0 + 2) + 2b_n^2)]$$

Therefore, the new expressions of A and B are shown in Eqs. (43) and (44).

$$A = H_1 + iH_2 = \left[\left(\frac{1}{2} + F_1 \right) a_0 b_0 + \left(\frac{1}{2} + G_1 \right) a_d b_d \right] \omega^2 + \left[\left(\frac{1}{2} + F_1 \right) a_0 b_0 b_p b_d + \left(\frac{1}{2} + G_1 \right) a_d b_d b_p b_d \right] + i[(F_2 a_0 b_0 + a_2 a_d b_d) \omega^2 + (F_2 a_0 b_0 b_p b_d + G_2 a_d b_d b_p b_d)] \tag{43}$$

$$B = J_1 + iJ_2 = \left[\left(\frac{1}{2} + F_1 \right) a_0 b_0 (b_p + b_d) + \left(\frac{1}{2} + G_1 \right) a_d b_d (b_p + b_0) \right] \omega + i[F_2 a_0 b_0 (b_p + b_d) + a_2 a_d b_d (b_p + b_d)] \omega \tag{44}$$

After obtaining the expressions for A and B , Eq. (27) for the modulus at the bottom is reformulated as follows:

$$E_d^*(\omega) = \frac{(L_1 L_3 + L_2 L_4) + i(L_2 L_3 - L_1 L_4)}{L_3^2 + L_4^2} = R_1 + iR_2 \tag{45}$$

where $L_1 = CH_1 + DJ_1 - DH_2 + CJ_2$

$$L_2 = CH_2 + DJ_2 + DH_1 - CJ_1$$

$$L_3 = H_1^2 - H_2^2 + J_1^2 - J_2^2$$

$$L_4 = 2(H_1 H_2 + J_1 J_2)$$

Based on the elastic relation for top and bottom modulus shown in Eq. (2), the complex modulus at the top is shown as

$$E_0^*(\omega) = k^*(\omega) E_d^*(\omega) \tag{46}$$

The complex modulus at the top is determined as

$$E_0^*(\omega) = N_1 + iN_2 \tag{47}$$

$$N_1 = \frac{k_0 \omega^2}{\omega^2 + b_k^2} \left(\frac{L_1 L_3 + L_2 L_4}{L_3^2 + L_4^2} \right) + \frac{b_k k_0 \omega}{\omega^2 + b_k^2} \left(\frac{L_2 L_3 - L_1 L_4}{L_3^2 + L_4^2} \right)$$

$$N_2 = \frac{k_0 \omega^2}{\omega^2 + b_k^2} \left(\frac{L_2 L_3 - L_1 L_4}{L_3^2 + L_4^2} \right) + \frac{b_k k_0 \omega}{\omega^2 + b_k^2} \left(\frac{L_1 L_3 + L_2 L_4}{L_3^2 + L_4^2} \right)$$

The elastic equation for the center modulus can be derived from Eq. (1), which is shown as

$$E_c = \left(1 + \frac{k - 1}{2^n} \right) E_d \tag{48}$$

Thus, the complex modulus at the center is calculated as

$$E_c^*(\omega) = \left(1 + \frac{k^*(\omega) - 1}{2^{n^*(\omega)}} \right) E_d^*(\omega) \tag{49}$$

Therefore, using the accurate Laplace transforms for n and k and the complex modulus at the bottom shown in Eq. (45), the complex modulus at the center is determined as



$$E_c^*(\omega) = (M_1 R_1 - M_2 R_2) + i(M_2 R_1 + R_1 R_2) \quad (50)$$

$$\text{where } M_1 = \frac{2f(\omega^2 + b_k^2) + p(k_0\omega^2 - 1) + q(b_k k_0\omega)}{2f(\omega^2 + b_k^2)}$$

$$M_2 = \frac{q(k_0\omega^2 - 1) - p(b_k k_0\omega)}{2f(\omega^2 + b_k^2)}$$

$$p = \cos[\ln(2)g]$$

$$q = -\sin[\ln(2)g]$$

$$f = \frac{n_0\omega^2}{\omega^2 + b_n^2}$$

$$g = \frac{b_n n_0 \omega}{\omega^2 + b_n^2}$$

References

- AASHTO (2008) Mechanistic-empirical pavement design guide. A manual of practice, interim edition. American Association of State Highway and Transportation Officials: Washington
- Al-Azri NA, Jung SH, Lunsford KM, Ferry A, Bullin JA, Davison RR, Glover CJ (2006) Binder oxidative aging in Texas pavements: hardening Rates, hardening Susceptibilities, and the impact of pavement depth. *Transp Res Board* 0361–1981
- AASHTO (2006) Standard specification for mixture conditioning of hot mix asphalt (HMA). AASHTO R30-02: Washington
- Braham AF, Buttlar WG, Clyne TR, Marasteanu MO, Turos MI (2009) The effect of long-term laboratory aging on asphalt concrete fracture energy. In: *Asphalt Paving Technology: Association of Asphalt Paving Technologists-Proceedings of the Technical Sessions*
- Farrar M, Harnsberger P, Thomas K, Wisner W (2006) Evaluation of oxidation in asphalt pavements test sections after four year of service. Paper presented at the International Conference on Perpetual Pavement, Western Research Institute
- Luo R, Lytton RL (2012) Selective absorption of asphalt binder by limestone aggregates in asphalt mixtures. *J Mater Civil Eng* 25(2):219–226
- Underwood BS, Kim YR (2012) Microstructural association model for upscaling prediction of asphalt concrete dynamic modulus. *J Mater Civil Eng* 25(9):1153–1161
- Kutay M, Gibson N, Youtcheff J, Dongré R (2009) Use of small samples to predict fatigue lives of field cores: newly developed formulation based on viscoelastic continuum damage theory. *J Transp Res Board* 2127:90–97
- Park H, Kim YR (2013) Investigation into top-down cracking of asphalt pavements in North Carolina. *Transp Res Board* 2368:45–55
- NCHRP 1-37A (2004) Guide for mechanistic-empirical design of new and rehabilitated pavement structures. National cooperative highway research program, transportation research board, national research council, Washington
- Luo X, Luo R, Lytton RL (2013) Characterization of asphalt mixtures using controlled-strain repeated direct tension test. *J Mater Civil Eng* 25(2):194–207
- NF EN 12697-26 (2004) Bituminous mixtures: test methods for hot mix asphalt—Part 26: Stiffness
- Glover CJ, Liu G, Rose AA, Tong Y, Gu F, Ling M, Arambula E, Estakhri C, Lytton RL (2014) Evaluation of binder aging and its influence in aging of hot mix asphalt concrete: Technical Report. Publication FHWA/TX-14/0-6613-1. Texas A&M Transportation Institute, College Station
- Levenberg E, Uzan J (2004) Triaxial small strain viscoelastic-viscoplastic modeling of asphalt aggregate mixes. *Mech Time Depend Mater* 365–384
- Luo R, Lytton RL (2009) Characterization of the tensile viscoelastic properties of an undamaged asphalt mixture. *J Transp Eng* 136(3):173–180
- Koohi Y, Lawrence JJ, Luo R, Lytton RL (2012) Complex stiffness gradient estimation of field-aged asphalt concrete layers using the direct tension test. *J Mater Civil Eng* 24(7):832–841
- Schapery RA (1994) Correspondence principle and a generated J integral for large deformation and fracture analysis of viscoelastic media. *Int J Fract* 25(3):195–223
- Zhang Y, Luo R, Lytton RL (2012) Characterizing permanent deformation and fracture of asphalt mixtures by using compressive dynamic modulus tests. *J Mater Civil Eng* 24(7):898–906
- Luo X, Luo R, Lytton RL (2015) Mechanistic modeling of healing in asphalt mixtures using internal stress. *Int J Solids Struct* 60:35–47
- Luo X, Zhang Y, Lytton RL (2016) Implementation of pseudo J-integral based Paris' law for fatigue cracking in asphalt mixtures and pavements. *Mater Struct* 49(9):3713–3732
- Findley WN, Lai JS, Onaran K (1989) Creep and relaxation of nonlinear viscoelastic materials: with an introduction to linear viscoelasticity. Dover Publications, New York
- Schapery RA (1961) Two simple approximate methods of Laplace transform inversion for viscoelastic stress analysis. Guggenheim Aeronautical Laboratory, California Institute of Technology, Pasadena

